Inscription and characterization of waveguides written into borosilicate glass by a high-repetition-rate femtosecond laser at 800 nm

Thomas Allsop,* Mykhaylo Dubov, Vladimir Mezentsev, and Ian Bennion
Photonics Research Group, Aston University, Aston Triangle, Birmingham B4 7ET, United Kingdom
*Corresponding author: t.d.p.allsop@aston.ac.uk

Received 1 October 2009; revised 8 February 2010; accepted 4 March 2010;
posted 16 March 2010 (Doc. ID 118030); published 29 March 2010

A series of waveguides was inscribed in a borosilicate glass (BK7) by an 11 MHz repetition rate femtosecond laser operating with pulse energies from 16 to 30 nJ and focused at various depths within the bulk material. The index modification was measured using a quantitative phase microscopy technique that revealed central index changes ranging from 5×10^{-3} to 10^{-2}, leading to waveguides that exhibited propagation losses of 0.2 dB/cm at a wavelength of 633 nm and 0.6 dB/cm at a wavelength of 1550 nm with efficient mode matching, less than 0.2 dB, to standard optical fibers. Analysis of the experimental data shows that, for a given inscription energy, the index modification has a strong dependence on inscription scanning velocity. At higher energies, the index modification increases with increasing inscription scanning velocity with other fabrication parameters constant. © 2010 Optical Society of America

OCIS codes: 140.7090, 230.7390.

1. Introduction

Since the initial demonstration of the use of a femtosecond laser to produce waveguides in glassy materials [1] there has been increasing interest in using this technology to fabricate optical devices both in fiber and planar optic configurations and in various kinds of glasses, such as fused silica and doped and borosilicate glasses [2–7]. Because of the possibility of inscribing three-dimensional structures with this technique, there is growing interest in the fabrication and performance of waveguides and other devices in borosilicate glasses, which are widely used in commercial optics due to the existence of well-established manufacturing procedures. These procedures result in low processing cost along with good chemical stability and high transmission in the visible and near-infrared spectrum. Some researchers have reported the fabrication of waveguides in borosilicate glasses, but with relatively high attenuation coefficients of around 1 dB cm^{-1} and above at 1300 nm [4–8], with only a few research groups demonstrating low-loss optical waveguides in BK7 glass possessing attenuations of around 0.3 dB cm^{-1} at 1550 nm [9]. The low-loss waveguides were produced using a 1 MHz repetition rate laser, but the reports lack detail of the induced index. Reference [9] also implies that high-repetition-rate systems produce lossy waveguidelike structures.

In this paper we investigate the operational parameters that are required to fabricate low-loss waveguides using an 11 MHz repetition rate 800 nm femtosecond laser and obtain minimal propagation losses of 0.2 dB/cm at a wavelength of 633 nm and 0.6 dB/cm at a wavelength of 1550 nm. Our fabrication technique produces complex morphological waveguide structures that contain both positive and negative refractive index changes within one inscribed waveguide. The results are compared to those of other research groups using different inscription parameters (i.e., wavelength, pulse energy and repetition rate) and we show that similar energy densities are required to produce low-loss waveguides, suggesting that the amount of energy delivered to the glass is

0003-6935/10/101938-13$15.00/0

important and not the system that delivers that energy.

2. Fabrication of the Waveguides

A series of 50 nm waveguides was fabricated in planar samples of borosilicate glass; BK7 [supplied by UQG (Optics) Ltd] measuring 50 mm × 50 mm× 1 mm. Within each sample, three parameters were varied. First, pulse energy at the point of inscription ranged from 16.4 to 29.5 nJ in increments of 3.2 nJ. This energy range was chosen after some initial trials on BK7 with energies from 13.1 to 42 nJ, where it was found that the higher energies produced damage tracks, including voids. Second, three depths of inscription were used: 45, 60, and 75 μm. Again, this range was chosen after some preliminary trials at various depths. Third, the speed of inscription (and hence the optical fluence) was varied over the range of 20 to 60 mms^{-1}, with an incremental increase in speed of 5 mms^{-1} for each waveguide. In addition, the polarization of the inscribing light was changed relative to the direction of the scanning laser beam. Two linear air-bearing stages were used for the x, y directions (Aerotech Ltd Model ABL15000) and a linear motorized stage for the z direction (Aerotech Ltd Model BMS60 UFA).

The laser used for inscription was an 800 nm Femtosource laser [10], which is pumped with a Verdi 10 W green, 532 nm laser. The repetition rate of the femtosecond laser is 11 MHz. The temporal pulse widths of individual pulses were measured using a frequency-resolved optical gating technique (Newport, ultrashort laser pulse measurement device, Model UPM-8-50) and it was found that the pulse width could be varied depending on the adjustment of the laser mirrors and dispersive elements in the oscillator. A pulse width of 52 fs was chosen, that being the shortest pulse width obtainable with a reasonably radially symmetric beam profile (observed with a Thorlabs beam profiler, Model BP109-VIS). For this pulse width, the spectral bandwidth was 34 nm (observed with an Ocean Optics, QE65000 spectrometer).

The optical and mechanical schematic arrangement of the elements used for waveguide inscription is shown in Fig. 1.

The alignment and the required inscription depth are achieved by using a helium–neon laser and camera. The red light from this laser is projected through the objective lens on to the sample to be inscribed, which is mounted on a tip/tilt stage. The back reflection of the red light from the surface of the sample is monitored with the camera and brought into focus on the surface of the sample by adjusting the z-axis translation stage. To ensure that the sample's top surface is flat and stays at the focal point of the objective lens, several points on the surface of the sample are chosen to be monitored and the tip/tilt stage is adjusted to maintain the focal point over the entire sample's surface; see Fig. 1(b). Control of inscribing optical fluence and the polarization state is achieved by the use of a half-wave plate to adjust the azimuth and a linear polarizer used as an attenuator. We define the X-polarization as being perpendicular and the Y-polarization as parallel to the direction of scanning; see Fig. 1(a).

Several objective lenses were used to produce waveguides in the BK7 glass. After some preliminary trials aimed at producing smooth, nondamaged tracks with no voids, it was decided to use an objective with an NA of 0.80 and magnification of 60. It was observed during fabrication of the waveguides in the BK7 glass that femtosecond pulse energies above 19.4 nJ produced a continuum light within the material, which became more significant with increasing scanning velocities for a given pulse energy, suggesting more material processing was occurring.

After the completion of the inscription of 240 X-polarization and 240 Y-polarization waveguides, the samples were visually inspected with a differential interference contrast microscope. Some index modification features similar to those in Ref. [11] were observed, but at lower pulse energies; see Fig. 2(A). Also, various morphologies of index change were observed depending on the inscription parameters; again, examples are shown in Fig. 2(A).

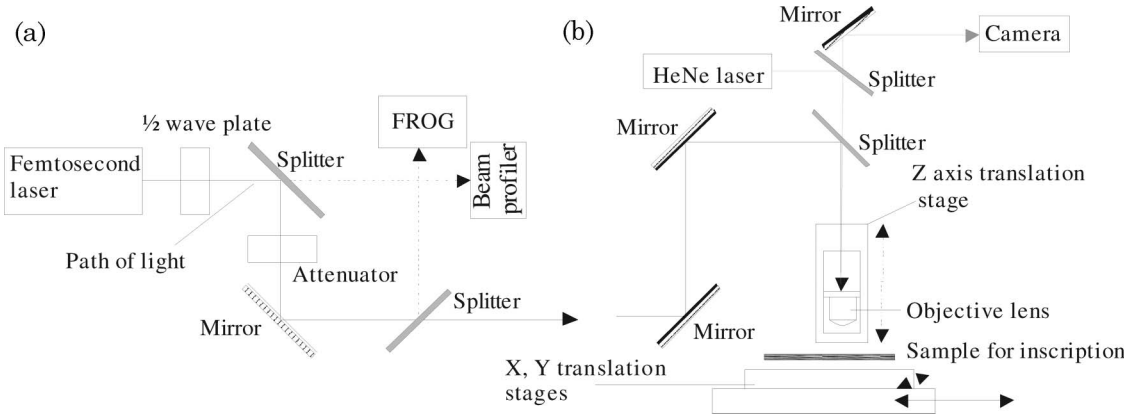

Fig. 1. Optical and mechanical schematic of the inscription apparatus. (a) Overhead view of the light source and diagnostics. (b) Side view of the focusing and inscription equipment.

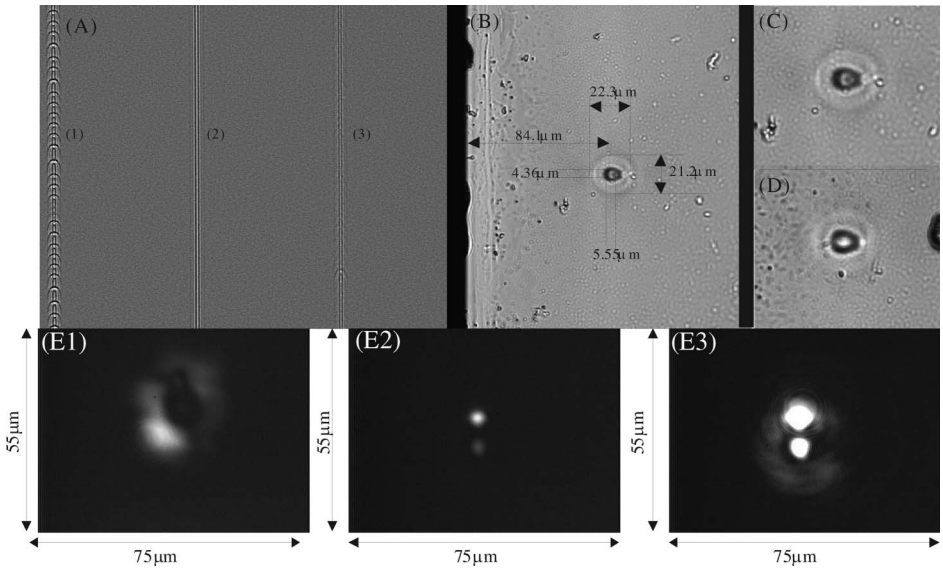

Fig. 2. Microscope images of example fabricated waveguides. (A) Examples of the overhead views of three waveguides with the same inscription energy of 16.4 nJ and with scanning speeds of (1) 25 and (2) 30 mms^{-1} inscribed from top to bottom, and (3) 30 mms^{-1} inscribed from bottom to top at a depth of 45 μm. (B) Example of the cross section of a waveguide with an inscription energy of 29.4 nJ with a scanning speed of 25 mms^{-1}. (C) Close-up of the waveguide in (B). (D) Waveguide written with the same sample inscription conditions, but with opposite scan direction. (E1), (E2), (E3) examples of the various modes of a fabricated waveguide observed in the near field at a wavelength of 633 nm. Fabrication conditions for this waveguide were inscription energy 19.6 nJ, depth of waveguide 72 μm, scan velocity 45 mms^{-1}, with measured waveguide characteristics of maximum Δn, 1.2×10^{-3}; V parameter, 2.4; and attenuation coefficient, 0.5 dB cm^{-1} at 633 nm.

The planar BK7 samples were cut in half using a diamond band saw (Logitech Model 15 diamond wire and disc saw), bisecting all the waveguides and producing two sections from the one sample, each having a length of 2.2 cm. Second, the cut faces of the two sections were lapped and polished (Logitech PM5 precision lapping and polishing machine); examples are shown in Figs. 2(B), 2(C), and 2(D). The end faces were visually inspected with a microscope and the inscribed structures were found to be reasonably radially symmetric. Also, the waveguiding properties were investigated by illuminating the structures with a 633 nm light source and they were found to support several modes; examples are shown in Figs. 2(E2), 2(E2), and 2(E3).

All the sample waveguides were inspected using the quantitative phase microscopy (QPM) method [12,13], from which a cumulative index profile over the radial distance from the central axis of the waveguide can be obtained. The peak cumulative index change in the inner and outer regions of the waveguide and the effective diameters of the two modified regions of the waveguide are defined in Fig. 3(a).

The radial refractive index profiles of the waveguides were reconstructed from the cumulative phase data obtained from QPM using the Abel

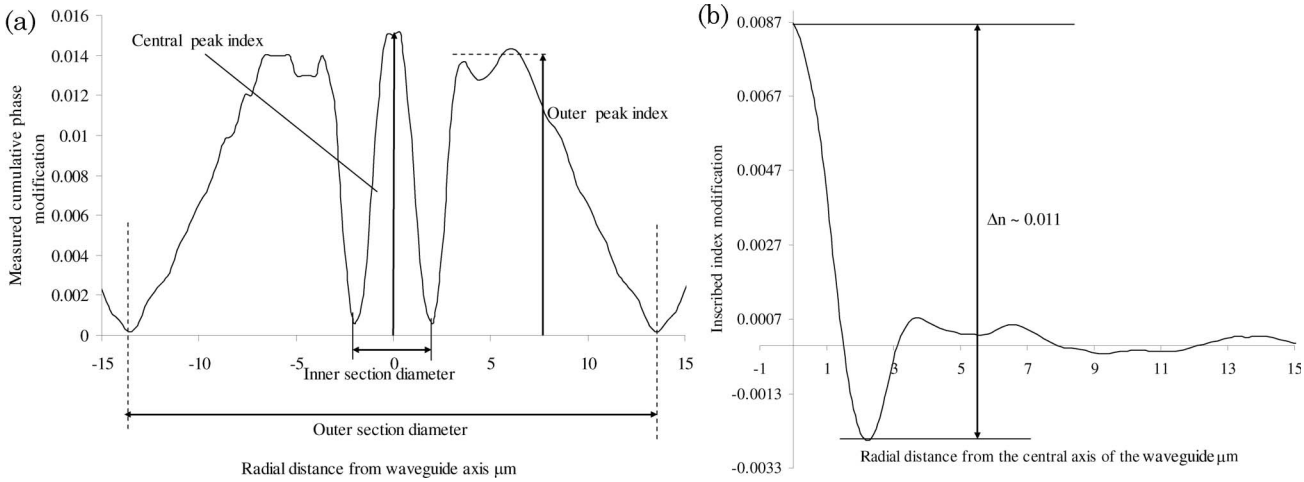

Fig. 3. (a) Typical cumulative phase profile obtained from QPM defining the measurements taken from the data. The waveguide was written with X-polarized light, an energy of 19.6 nJ, scanning velocity of 55 mms^{-1}, and at an approximate depth of 55 μm. (b) Calculated radial index profile of the waveguides using an Abel inverse transform.

inverse transform method [12,13]. To implement an Abel transform, it must be assumed that the waveguide is radially symmetric about its axis. A visual inspection of the cross section of the waveguides suggested this to be a reasonable assumption; see Fig. 2(B). The reconstruction produced some complex refractive index profiles, incorporating both increases and decreases in refractive index. It was also was found that the changes of refractive index were approximately the same for both polarization states, although there were some minor differences observed. A typical example of the results obtained from this reconstruction is shown in Fig. 3(b). The waveguides' ellipticities (defined as $1 - a/b$, where a and b are the major and minor semi-axes) were measured for both polarizations and were found to range from $+0.07$ to -0.07.

By using the defined radial diameter parameters for the index modification shown in Fig. 3, it was found that the polarization of the inscribing beam had negligible effect on the overall size of the cumulative index modification for a given scanning speed; an example is shown in Fig. 4. The error associated with the measurement of the inner section of the waveguide is $\pm 0.3\,\mu$m and that for the outer section is $\pm 1.2\,\mu$m; these values are determined by the minimum step size of the QPM technique used, the estimate of the minimum of the inner index modification, and the estimate of the total width of the outer section of the waveguide; see Fig. 3.

Figure 5 shows the peak index modifications obtained for the waveguides fabricated with the femtosecond laser with both polarization states of the laser. These data include results obtained for different inscription conditions (both inscription energies and scanning velocities) at a depth of $70\,\mu$m from the surface of the glass. By inspecting Fig. 5, it may be seen that the results for the same inscription energy are clustered together; within these groups, the scanning velocities increase from 30 to 60 mms^{-1} with increasing sample number on the x axis.

The associated index error has not been added to the graph, so the graph is easier to inspect visually. The error in the refractive index measurement is $\pm 1.3 \times 10^{-4}$, which comes from the inaccuracy of the QPM method via the Abel inverse transform. Inspection of Fig. 5 shows that the peak index clearly increases with pulse energy and there is evidence that the index also grows with increasing scanning velocity. More specifically, for an increase in the pulse energy (in this energy range), there is an increase in the peak index change in the inner and outer regions of the waveguide for both X- and Y-polarization states of the laser. The maximum index change observed was 10^{-2} for inscription energy of 29.4 nJ for both polarization states, but, at this energy, there were variations in the index value ranging from 4×10^{-3} to 1.0×10^{-2} (discussed in the following sections).

While the measured attributes of the waveguides were approximately the same, there are some differences observed in the cumulative index morphology for the two polarization states of the inscribing beam. This difference may be explained by the small but significant ellipiticity of the inscribing beam profile, with the Y semi-major axis having a slightly larger radius than the X semi-major axis in the scanning direction. Thus, the X-polarized light (perpendicular to the scan direction) delivers slightly less overall energy to the waveguide than the Y-polarized light (parallel to the scan direction). Along with the Fresnel reflection losses at the sample's surface being

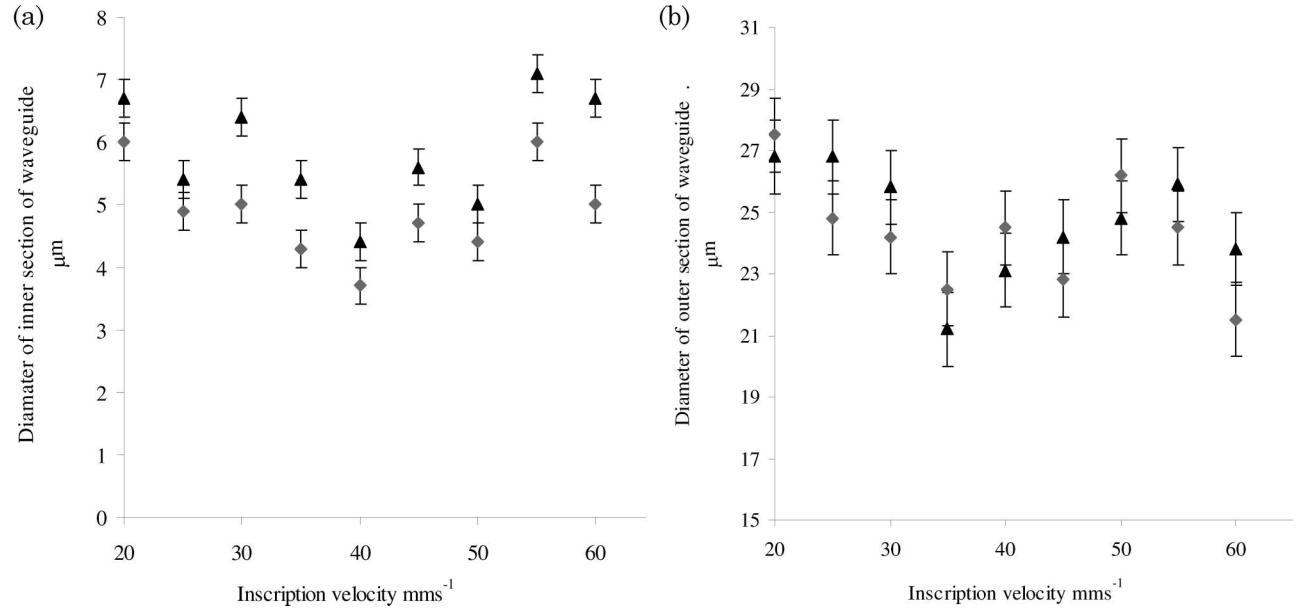

Fig. 4. Example of the comparison of the radial diameter of the index modification as a function of scanning inscription velocity: (a) the inner section and (b) the outer section of the waveguide. The inscription energy was 29.4 nJ, the depth was $43\,\mu$m, and both polarization states are shown (X-polarization, ◆; Y-polarization, ▲).

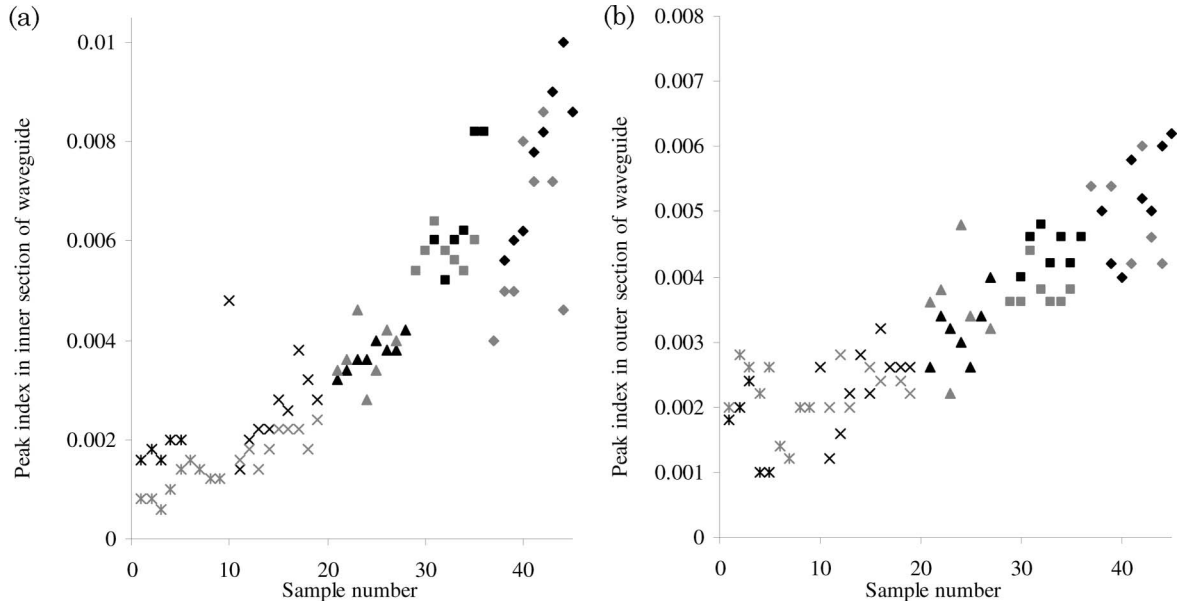

Fig. 5. pi twb 0.3w Peak index modification estimated by the use of QPM and the inverse Abel transform for (a) inner regions and (b) outer regions for all waveguides fabricated with both polarization states of the inscribing beam (black shapes for Y-polarization, gray shapes for X-polarization), at a depth of 70 μm and various inscription pulse energy groups (∗, 16.4 nJ; ×, 19.6 nJ; ▲, 22.9 nJ; ■, 26.1 nJ; ◆, 29.5 nJ). Within each energy group, the results are presented in order of increasing inscription scanning velocity with increasing sample number.

slightly higher for X-polarized light, this may account for the observed differences in morphology.

The effects of inscription depth and scanning velocity on the index modification were also investigated at specific pulse energies for both polarization states. From Fig. 6, it may be seen that there is some difference between the two polarization states of the laser. The differences observed may be partly explained by the fact that, for a given objective lens (i.e., the focal length), there is an optimum inscription depth for a given material and an optimum energy. Away from optimum depth it has been found that positive index change decreases away from the optimum focal depth of the lens for a given inscription energy. Also, varying the inscription energy density changes the optimum inscription depth. We know that the inscription beam is elliptic and, thus, the laser operating with Y-polarized light delivers higher energy density into the material, thereby changing the optimum depth to produce maximum index change. If more energy is being delivered into the material, there is a higher overall temperature rise of that material, which affects the refractive index of the material via the thermo-optic effect, which, in turn, modifies the effective focal length.

Inspecting the magnitude and extent of the index modification as a function of scanning velocity for a given inscription energy (Figs. 7 and 8), it appears that, for both polarization states of the laser, increasing the scanning velocity increases the peak index modification for both inner and outer regions for inscription energies of 18 nJ and above, with this effect increasing with higher inscription energies. At inscription pulse energies below 18 nJ, the inner index modification still increases with an increase in scanning velocity, though to a lesser extent, but the outer

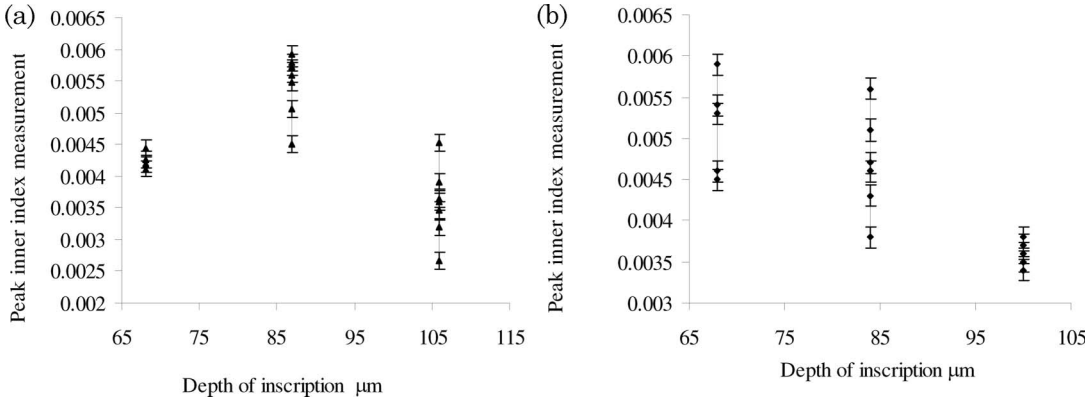

Fig. 6. Examples of the peak index change as a function of inscription depth at an inscription energy of 22.9 nJ for both (a) X- and (b) Y-polarization states at three different depths: (a) depths of 68, 87, and 106 μm, and (b) depths of 68, 84, and 100 μm.

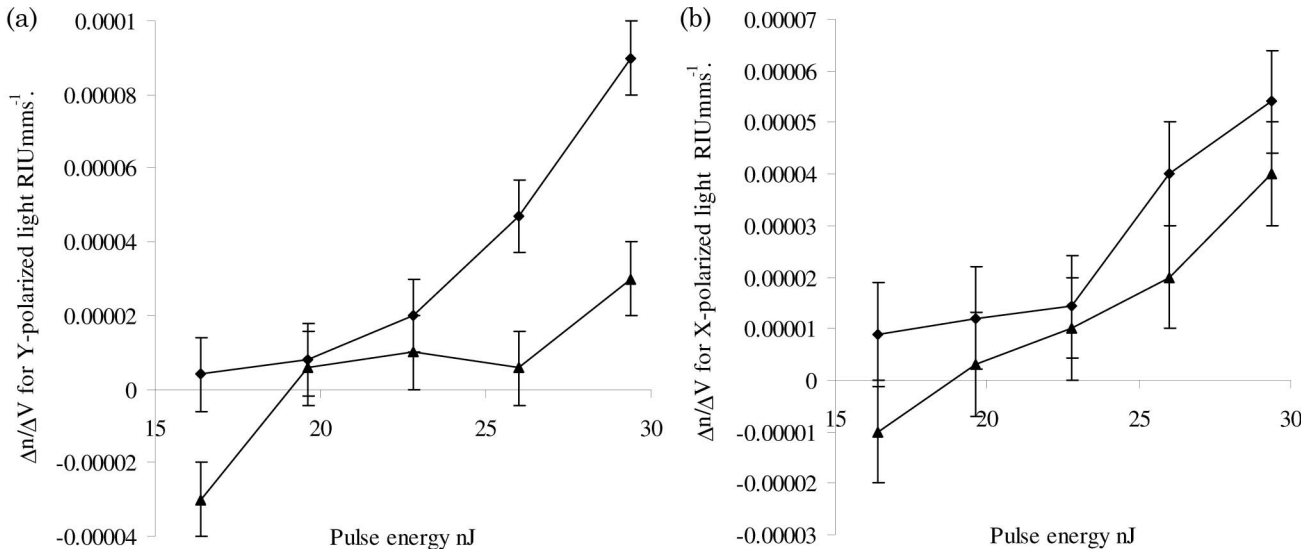

Fig. 7. Rate of index change (Δn) with respect to scanning velocity (ΔV) as a function of inscription energy (◆, the inner index feature; ▲, the outer index feature. (a) Y-polarization and (b) X-polarization. The lines are simply added to link together points relating to the same index feature as an aid to the eye.

index modification decreases. This increase in refractive index with scanning velocity can be seen from a close inspection of Fig. 5 as, within each energy group, inscription scanning velocity increases with sample number. To illustrate this behavior over all the experimental data, Fig. 7 shows experimentally measured ratios of change in the index modifications with respect to scanning velocity ($\Delta n_c/\Delta v$) as a function of inscription energy (the errors in index in Fig. 7 come from the QPM technique combined with the uncertainty in the linear regression to the data sets shown in Fig. 5).

There are several possible reasons why this behavior is exhibited. During the fabrication of the waveguides, it was observed that, for pulse energies above 19.4 nJ, the creation of a laser-induced continuum became stronger with increasing scanning velocities. This behavior indicates that, at higher scanning velocities, less energy is being used in the inscription process, implying that there are smaller scattering losses from the inscribing beam at higher scanning velocities, which would contribute to an overall increase in index modification. It was also observed that, for increasing energy, there was a reduction in the size of the central index feature of the waveguide; this has been reported by others who have seen index modification morphology similar to Fig. 3 and attributed this to a thermal lensing effect [14–16].

It is also known that cooling rates have an effect on the refractive index of glass [4,17]. At much higher cooling rates than conventional quenching processes, the structure of the glass that exists at high temperatures is fixed in the material by the cooling processes [17]. It may be that, with an increase in the scanning velocity, there is an increase in the cooling rate of the

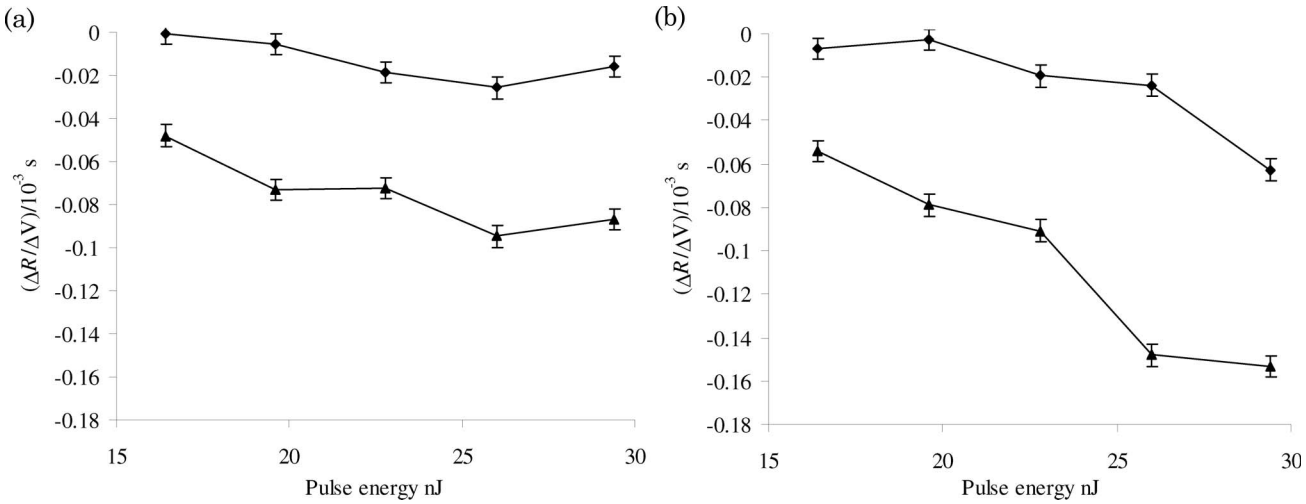

Fig. 8. Rate of change of the size of the index feature (ΔR) with respect to scanning velocity (ΔV) as a function of inscription energy (◆, the inner index feature; ▲, the outer index feature). (a) Y-polarization and (b) X-polarization.

postprocessed glass, which then would affect the index modification, as discussed below.

During inspection of the experimental data, it was noticed that, with an increasing scan velocity and energy, the cumulative refractive index modification radial size of both inner and outer features of the waveguide decreased. To illustrate this behavior, Fig. 8 shows experimentally measured ratios of change in the cumulative index modifications radial size to change in scanning velocities ($\Delta R/\Delta v$) as a function of inscription energy. The X-polarization operation of the inscription schemed a twofold reduction in radial size of the inner and outer index features compared with Y-polarization operation. This result suggests that less energy is being used for inscription in the X-polarization state (to the direction of the scanning beam) and, again, this can be explained, in part, by the ellipticity of the inscribing beam, which has a larger semi-axis in the Y direction.

To understand the observed index increase with increasing scanning velocity (with the same depth and pulse energy), we present a model of the heating dynamics during the process of femtosecond inscription at a high repetition rate. The purpose of this modeling is to determine the scanning velocity dependence of the cooling rate at the rear front of the heating wave produced by successive laser pulses as an aid to explain the experimental observations. It is well established [17] that the amount of modification of refractive index during the glass melt transition to a solid state at the so-called glass transition temperature T_g monotonously depends on the glass cooling rate at this point. We perform our analysis in the framework of the thermal conductivity equation with a moving heat source. While being the simplest possible model, it includes the appropriate heating and cooling processes of the material being used for waveguide fabrication. We use the thermal conductivity equation for the glass temperature, T, in the form

$$c\rho\frac{\partial T}{\partial t}-\kappa\Delta T=q(z-vt,r_\perp,t), \tag{1}$$

where $c=800\,\mathrm{J/kg/K}$ is the specific heat, $\rho=2500\,\mathrm{kg/m^3}$ is the glass density, $k=1\,\mathrm{WK/m}$ is the thermal conductivity, $\partial T/\partial t$ is defined as the rate of change of the temperature of the material with time, and v is the scanning velocity. The values of all these parameters are given for BK7 glass in Ref. [18]. Equation (1) is written in the glass coordinate frame where the heat source and a distribution of temperature are moving at constant velocity v. Since the repetition rate exceeds the material relaxation rates by at least 3 orders of magnitude, it is natural to assume a heat source being stationary in the laboratory frame of coordinates. Hence, it is more convenient to consider this problem in this frame where both the heat source and the temperature are stationary:

$$-c\rho v\frac{\partial T}{\partial z}-\kappa\Delta T=q(z,r_\perp). \tag{2}$$

Equation (2) describes a stationary heat wave with a heating/cooling rate expressed locally as $v\partial T/\partial z$. It is natural to introduce dimensionless spatial variables z', $r_\perp{}'$ as $z=Rz'$ and $r_\perp=Rr_\perp{}'$, where R is a characteristic size of the heat source. Thus, the problem becomes dependant on only one parameter, $\mathrm{Pe}=vRc/\kappa$, which is known as a Péclet number [19]:

$$-\mathrm{Pe}\frac{\partial T}{\partial z}-\Delta T=\frac{R^2}{\kappa}q(z,r_\perp). \tag{3}$$

Because Eq. (3) is linear, the shape of the temperature profile will be determined by the shape of heat source q and the value of the Péclet number, Pe, and the amplitude of the temperature profile will be scaled with that of the heat source.

It was found from previous experiments [20] that the amount of absorbed energy per laser pulse is between 10% and 50%, which results in about 10 nJ for each of 10^4 pulses per second. Typically, the size of the absorbing domain is of the order of a couple of micrometers [20]. Hence, we assume that the heat source generates the heat at the rate of $q=10\,\mathrm{nJ}\times10^4/\mathrm{s}/(2\,\mu\mathrm{m})^3$. Equation (3) was solved numerically assuming for simplicity a spherical heat source. The results are presented in Figs. 9 and 10.

Figure 9 shows the distribution of glass temperature along the z axis in a heat wave. Each point on the axis is exposed to this wave, being initially heated and eventually cooled at the rear. The cooling rate of the sample at the glass transition temperature $T_g=570\,^\circ\mathrm{C}$ versus different Péclet numbers in the range between zero and 1.2 is shown in Fig. 10.

It is seen that cooling rate depends on the translation speed nonmonotonously. It initially increases with speed, before starting to fall off as the Péclet number approaches 1.2. Qualitatively speaking, the quicker the translation speed, the higher the cooling rate, which leads to a larger modification of refractive index.

Considering the index changes as a function of energy dose received by the BK7 glass, defined as [11]

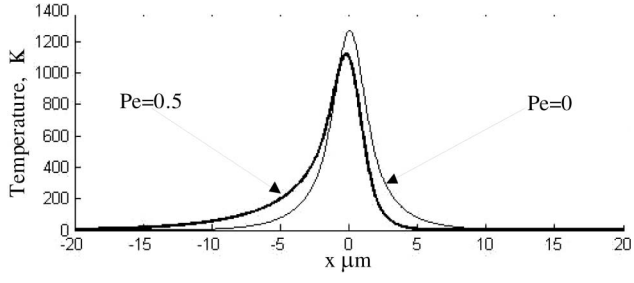

Fig. 9. Theoretically calculated temperature distribution of glass along the z axis in a heat wave for two Péclet numbers, assuming a Gaussian heat distribution with $2\,\mu\mathrm{m}$ being at the e^{-1} of the maximum value.

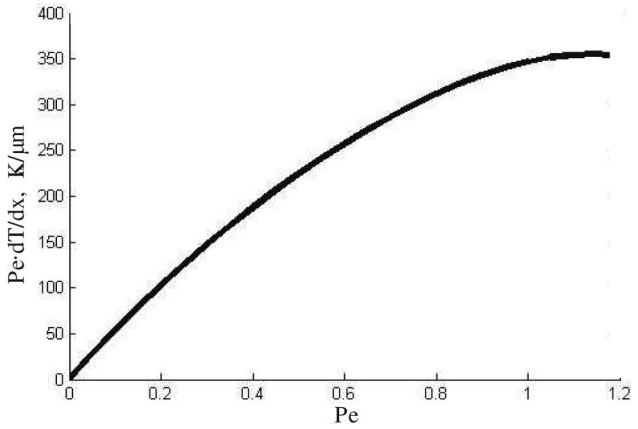

Fig. 10. Cooling rate of the sample at the glass transition temperature ($T_g = 570\,°C$) as a function of the Péclet number for BK7 glass, varying only the scanning velocity.

$$\text{Energy Dose} = \frac{E_{\text{pulse}} R_p}{AV}, \tag{4}$$

where E_{pulse} is the energy of the pulse from the laser, R_p is the laser repetition rate, A is the spot area of the laser, and V is the scanning velocity. By using this relationship, the data in Fig. 11 reveal that there is an optimum dosage of about $1\,\mu\text{J}\,\mu\text{m}^{-3}$ to produce maximum refractive index change, with an increasing dosage beyond this optimum producing a decrease in maximum refractive index change, as shown in Fig. 11. Separately, we also observed that a minimum dosage of around $0.5\,\mu\text{J}\,\mu\text{m}^{-3}$ was required to obtain a reasonable refractive index modification ($\sim 10^{-3}$); this applies to both polarization states of the laser. For a given objective lens, the energy dosage appears to be an important factor for peak index change, along with inscription depth, as shown in Fig. 6.

3. Optical Characterization of the Waveguides

After the planar BK7 samples were prepared (cut into two sections with the end faces lapped and polished), the samples were clamped to the support on a translation stage. A helium–neon laser (633 nm) was coupled to a pigtailed optical fiber, with the other end of the fiber being cleaved and cleaned. The cleaved end of the fiber was used to launch the light into the waveguide and a six-axis micropositioner was used to optimize the coupling from the fiber to the waveguide sample. This coupling alignment was achieved by viewing the sample and the fiber by microscope. The transmitted light from the waveguide was then collimated and focused (via two objective lenses) on an optical patch cord coupled to an optical spectrum analyzer, which is used to optimize the coupling of near-infrared (1550 nm) and 633 nm sources (narrow and broadband) into the waveguide sample. A camera is used to view the near-field modal profile of the emitted light, to check for single-mode or multimode operation of the waveguide. Also, the optical power is monitored and checked with a meter used in conjunction with an aperture to help differentiate the guided light from scattered light; see Fig. 12. The losses of the arrangement were also measured without the presence of a BK7 waveguide sample.

The following attenuation coefficient results assume a Fresnel loss of 4% per facet. It was also assumed that an additional loss would be incurred due to mode mismatch from the fiber to the 2.2 cm waveguides. This additional mode mismatch loss

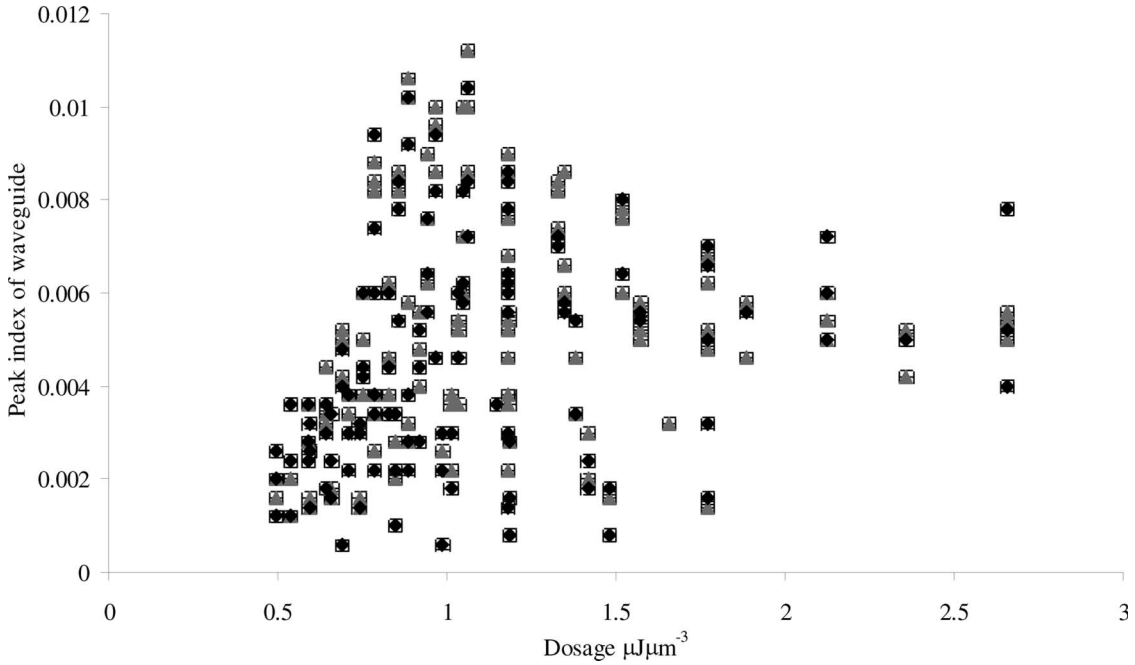

Fig. 11. Experimentally observed variation of modified index as a function of dosage for the laser operating in the Y-polarization state (♦) and the X-polarization state (▲), including all depths of inscription.

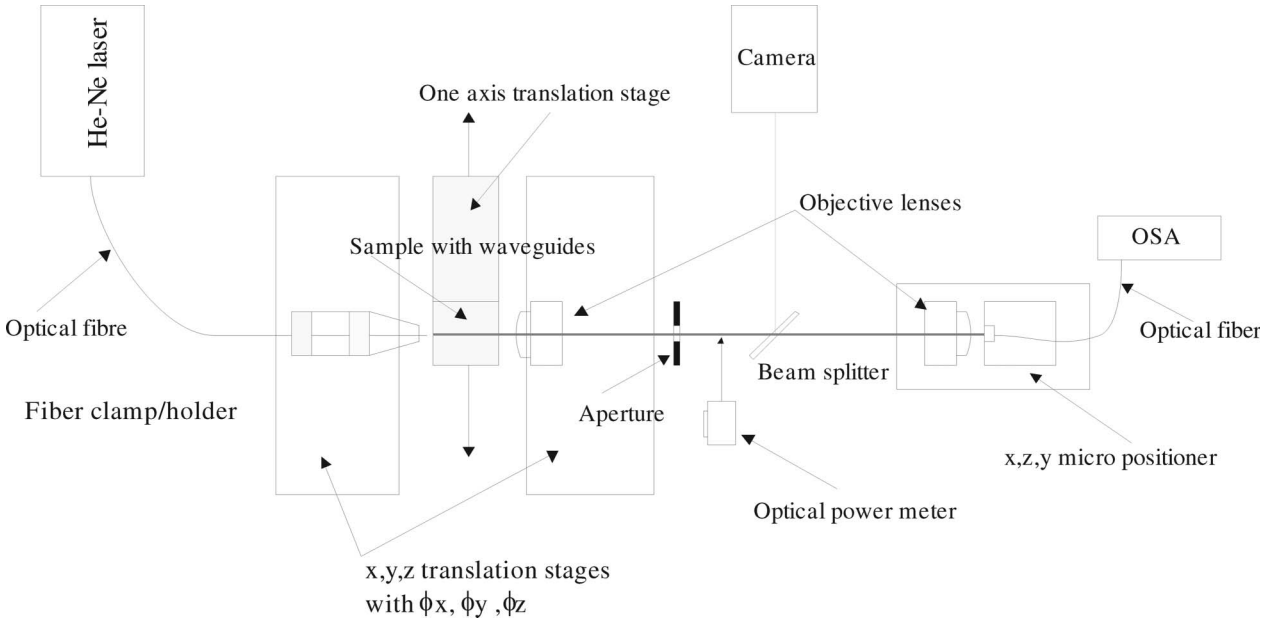

Fig. 12. Schematic of the apparatus used to obtain an estimate of the attenuation coefficient of the waveguides

was estimated at 2% for 633 nm light by coupling to a single-mode fiber and is a result of the fact that these waveguides are multimode at this wavelength.

During the procedure outlined above, inspection revealed three distinct types of waveguides, these being very low-scattering, high-scattering, and lossy (though weakly scattering) guides. Also, there appeared to be damaged waveguides with localized scattering centers, which is probably due to dust particles resting on the top surface of the BK7 glass sample during fabrication. All the values of the attenuation coefficients for both the X- and Y-polarization states are considered as a function of the V parameter and are shown in Figs. 13 and 14. The V parameter is estimated by $V = k_0 a n_p^2 \sqrt{2\Delta}$, with k as the free-space propagation constant, a as the effective waveguide radius, $\Delta = ({n_p}^2 - {n^2}_{\mathrm{BK7}})/2{n_p}^2$ with n_p as the peak refractive index of the waveguide, which is obtained from the QPM measurements in conjunction with the Abel inverse transform method,a and n_{BK7} as the refractive index of the BK7 sample.

The authors acknowledge that there is some uncertainty with the estimate of the peak refractive index.

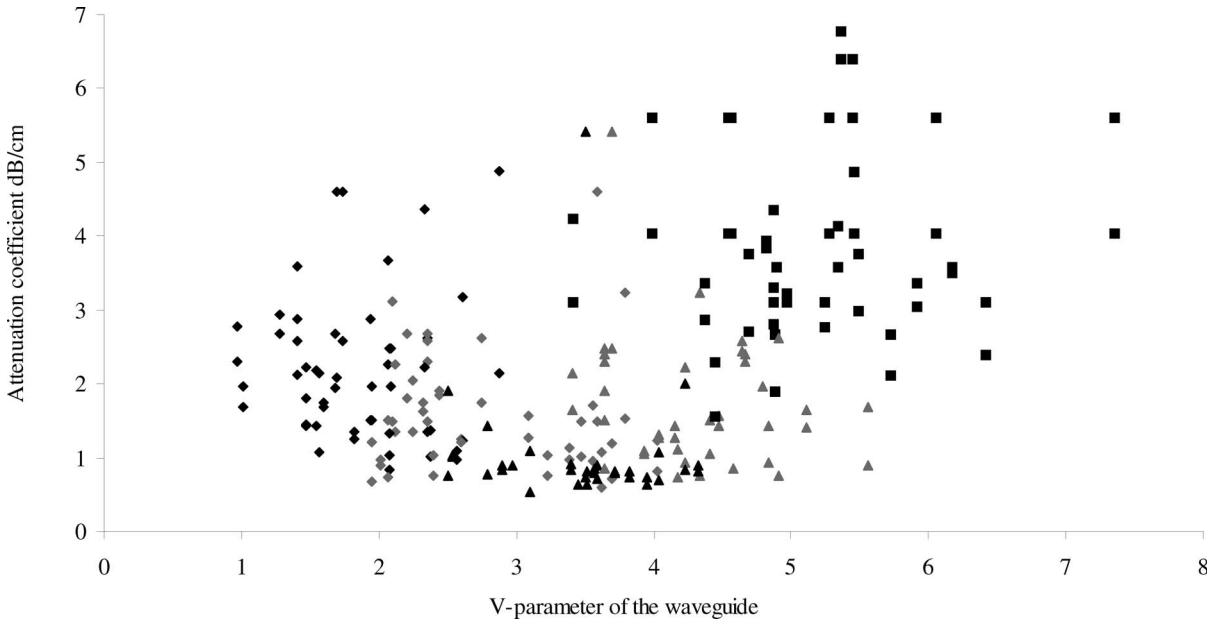

Fig. 13. Attenuation coefficient of the waveguides fabricated in a sample of BK7 with X-polarized femtosecond laser light as a function of their V parameters, indicating their inscription energy: black ◆, 16.4 nJ; gray ◆, 19.6 nJ; black ▲, 22.9 nJ; gray ▲, 26.1 nJ; and black ■, 29.5 nJ.

This error comes from the assumption underpinning the use of the Abel inverse algorithm: that the waveguide's cross section is radially symmetric. After inspecting the waveguide's cross section [for examples, see Figs. 2(C) and 2(D)] this appears to be a reasonable assumption. Furthermore, the form of the V parameters for the bound and leaky modes for a non-step-profile waveguide is more complex than the simple equation stated above [21]. Nevertheless, this still provides a reasonable estimate for the V parameter [21] of the femtosecond laser fabricated waveguides.

Inspection of Figs. 13 and 14 reveals that the minimum attenuation coefficients of the waveguides were around 0.5 and 0.2 dB/cm for the X- and Y-polarized light, respectively, where both V parameters were approximately 2.5 at a wavelength of 633 nm. The inscription energy for these low attenuation waveguides is approximately 20 nJ. The lower inscription energies produce the majority of waveguides with high attenuation coefficients that also have low V parameters (less than 2). These low V-parameter values suggest weakly guiding waveguides. The higher inscription energies used (26.1 and 29.5 nJ) lead to larger V parameters, but also increasing average attenuation coefficients above a V value of 3, suggesting that, in this regime, the energy is damaging the glass; i.e., creating more scattering centers and a less smooth index modification. This behavior may be expected because of the damage observed within the waveguides at higher inscription energies during preliminary trials to find the optimum range of inscription conditions. The V parameter for both polarization inscription regimes varies from 0.8 to 7.5, indicating that these waveguides are single mode or few modes at a wavelength of 633 nm, and this was observed in near-field mode distributions; see Figs. 2(E1), 2(E2), and 2(E3), for example. The calculated V parameter for the waveguides for a wavelength of 1550 nm ranged from 0.4 to 3.1, with the lower inscription energy yielding the lower values, which again suggests that these waveguides may be single mode and weakly guiding.

The inscription depths used, from about 40 to 80 μm, appeared to have a less significant effect on the quality of the waveguides than the inscription energy dosage. This can seem from Figs. 15(a) and 15(b), where the dosage required to obtain low-loss waveguides for Y-polarized light is approximately the same as for X-polarized.

From the accumulated data obtained with a light source at 633 nm, the lowest loss waveguides (inscription energy of 22.9 nJ) were also evaluated at a wavelength of 1550 nm. It was found that the attenuation coefficients at the longer wavelength were approximately 1 dB greater; see Fig. 16. This may be expected due to greater mode mismatch between the fiber illuminating the waveguide and the waveguide itself, which would appear as an overall increase in attenuation of the waveguide. The lowest loss waveguide at 1550 nm was 0.5 dB/cm.

In addition, a small number of the waveguides was illuminated with a broadband light source from 1200 to 1700 nm. It was found that the broad spectral response of the waveguides varied from a gradual loss increase over the wavelength range in some instances, to other cases, where there were specific spectral ranges with significant loss increases; this is being investigated.

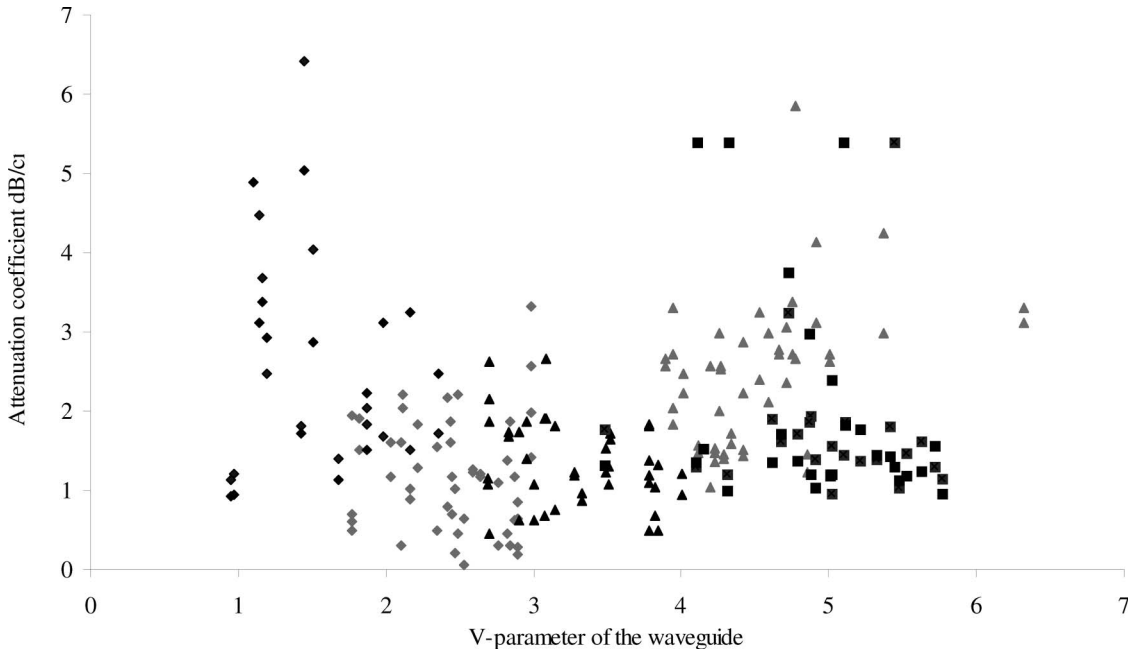

Fig. 14. Attenuation coefficient of the waveguides fabricated in a sample of BK7 with Y-polarized femtosecond laser light as a function of their V parameters, indicating their inscription energy: black ◆, 16.4 nJ; gray ◆, 19.6 nJ; black ▲, 22.9 nJ; gray ▲, 26.1 nJ; and black ■, 29.5 nJ.

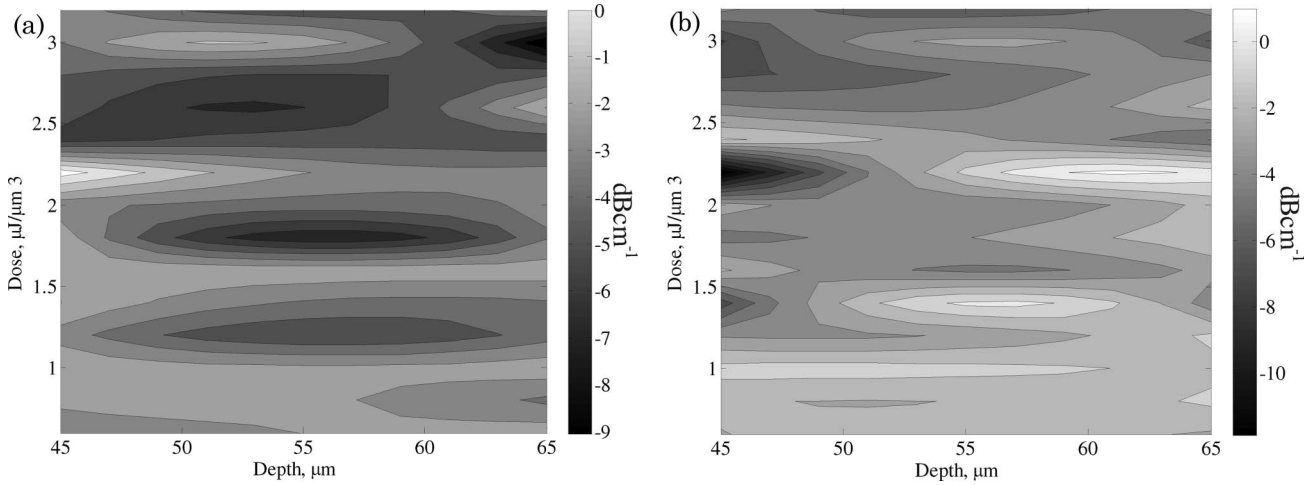

Fig. 15. (a) Effects of depth and dose on the overall attenuation coefficient of the waveguides at 633 nm for (a) Y-polarized inscription light and (b) X-polarized inscription light.

Small samples of the waveguides were illuminated with a pigtailed 1550 nm distributed feedback module laser, with some of the results shown in Fig. 16. It seemed there was an additional loss factor, but with the same trend curve for loss as a function of scanning velocity, for a given depth. This additional loss, in part, is assumed to be mode mismatch between the waveguide and SMF light source, leading to a measured lowest attenuation coefficient of ~0.5 dB/cm (assuming a higher level of mode mismatch, 1 dB) at a wavelength of 1550 nm for pulse energy of 22.9 nJ.

4. Discussion

There are several key observations that have come out of this study. Our results are best considered via a comparison with results obtained in borosilicate/BK7 glasses with different inscription systems. Reference [11] reports on a study of femtosecond inscription (pulse width ~300 fs) in a borosilicate glass similar to BK7 using a wavelength of 1045 nm and a repetition rate up to 5 MHz. First, in that study, the optimum inscription pulse energy is 75 nJ, which was capable of fabricating waveguides with an attenuation loss of 0.3 dB/cm at 1550 nm. This is comparable to the lowest loss waveguide at 1550 nm (0.5 dB/cm) fabricated with our 11 MHz system. In addition, our system produced waveguides with an attenuation coefficient of 0.2 dB/cm at a wavelength of 633 nm with inscription conditions of 19.6 nJ pulse energy, 35 mm/s scan velocity, and a 55 μm depth, which is comparable to Ref. [11].

A general inspection of the quality of waveguides fabricated with our system (see Figs. 13 and 14) suggests that the optimal pulse energy is between 19.6 and 22.9 nJ, with a scanning velocity between 35 and

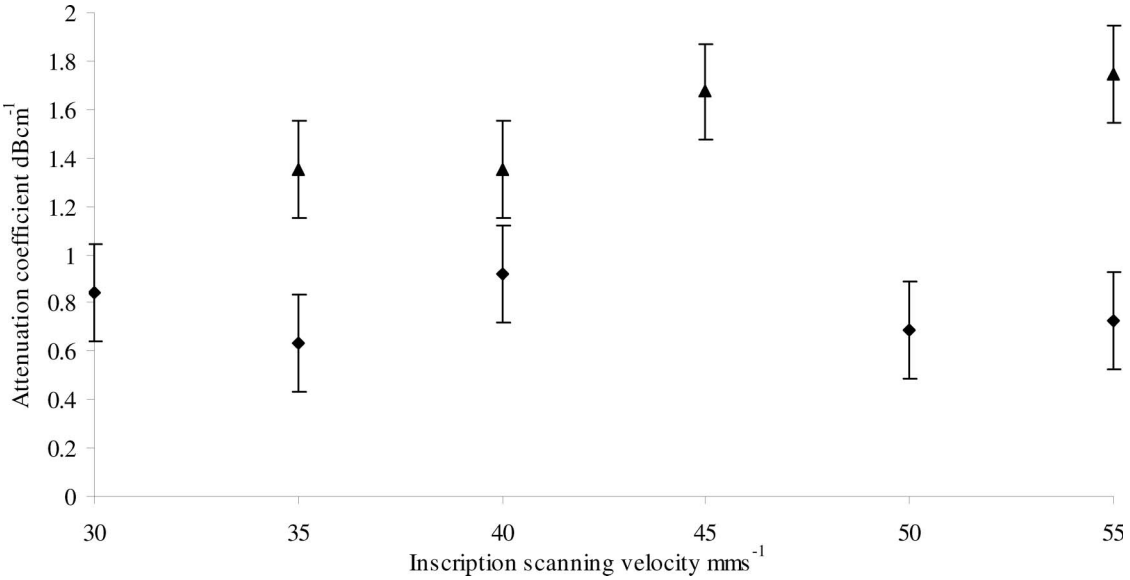

Fig. 16. Comparison of the measurements of the low-loss waveguides at 633 nm and at 1550 nm: ◆, losses at 633 nm and ▲, losses at 1550 nm. Fabrication conditions for this waveguide inscription energy 22.9 nJ, depth of waveguide 55 μm.

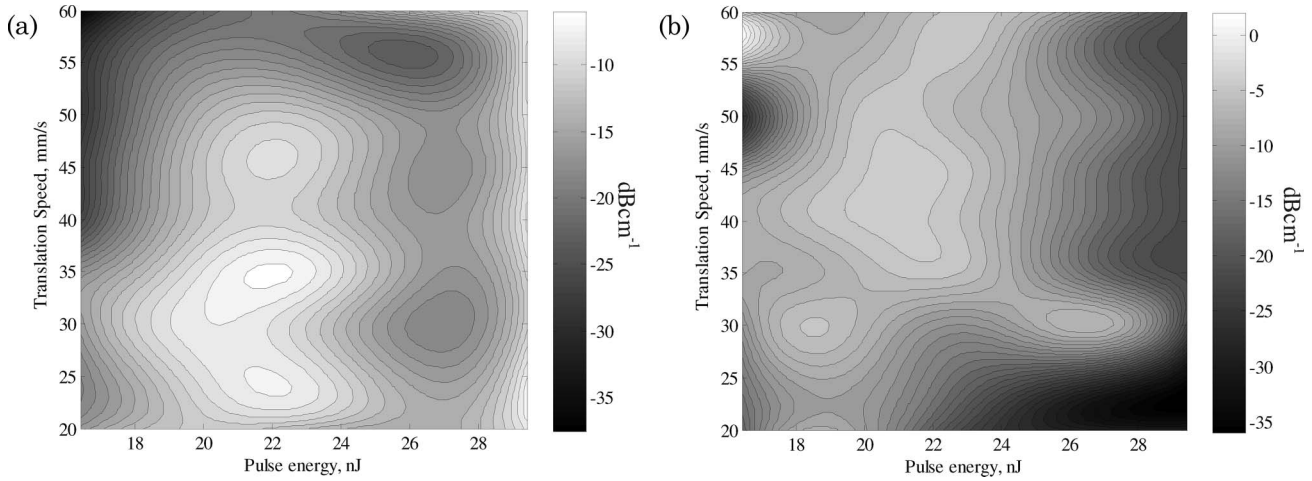

Fig. 17. Dependence on pulse energy and scanning speed of two sets of waveguide attenuation coefficients at a wavelength of 633 nm written with the femtosecond laser at a depth of 55 μm. (a) Y-linearly polarized and (b) X-linearly polarized.

45 mm/s for both linearly polarized states of inscribing light. This is summarized in Fig. 17, which provides results similar to those presented in Ref. [11]. It was found that, with higher average powers delivered to the sample, damage occurred, consisting of void formation in the central region of the waveguide while, at lower powers, very weak lossy waveguides were created. These results, along with results published in Ref. [11], indicate that, for a similar glass, there may be similar inscription conditions, regardless of the laser used for inscription, and that, in this heat accumulation regime, the amount of energy being delivered is more significant than the method used.

Inspection of Figs. 15 and 17 shows that the inscription conditions for optimal low-loss waveguides are very similar for both polarization states of the femtosecond inscribing laser. Other researchers have reported that polarization plays an important role in producing low-loss waveguides [14]. It should be noted that the laser they used had a 1 kHz repetition rate, pulse energies of up to 10 μJ, and was operated at a wavelength of 800 nm. While the index modification morphology appears to by slightly different from ours, as shown in Fig. 3, the inscription conditions for optimal waveguides appear to be very similar. Also, Fig. 11 shows that the peak index occurs for an energy dose of around 1 μJ μm^{-3} but, for optimal low-loss waveguides, the required dosage ranges from 0.6 to 1.2 μJ μm^{-3}, indicating that the index modification morphology also has a significant effect on the performance of the waveguides. Note that some waveguides were also fabricated with circularly polarized light, and initial observations of these waveguides showed little difference in index modification morphology compared to the two linear states of the femtosecond laser.

The physical characteristics of a typical low-loss waveguide (measured by white-light microscope and the QPM technique using the Abel transform) are an index change of 1×10^{-2} with a diameter of 3.6 μm for the central part, and an index change of 8×10^{-4} with a diameter of 19.2 μm for the outer part of the waveguide. One difference from the results given in Ref. [11] is that we obtained substantial changes in refractive index both negative and positive, with central index structure sizes ranging from 2 to 8 μm for pulse energies of 16.4 nJ and upward. We do have a higher repetition rate of 11 MHz, which leads to net fluence of 6 to 30 J cm^{-2} (using a lens with NA 0.8 and magnification of 60, with a focused beam waist of $\sim 2 \times 10^{-6}$ m), which is considerably lower than the net fluence of 2 kJ cm^{-2} stated in Ref. [11]. In making this comparison it must be kept in mind that we did use a different borosilicate/BK7 glass supplied by UQG (Optics) Ltd. The experimental data presented here and that in Ref. [11] suggest, assuming the index measurements are obtained by a similar method, that this behavior is very much material dependent.

It was also found that, for a given depth and pulse energy, both central and outer regions of the waveguide reduced in size with an increase in the scanning velocity; see Figs. 8(a) and 8(b). This trend appears to be consistent with other research groups' findings [3,11]. These measurements also suggest that index change increases with increasing scan velocity for a given pulse energy; see Figs. 5 and 7. To explain this, we considered a simplistic model consisting of only heat accumulation and thermal diffusion and calculated the rate of change of temperature with respect to time, finding that this increased at higher scanning velocities, and it is know that an increase in cooling rate increases the index modification [4,17].

References

1. K. M. Davis, K. Miura, N. Sugimoto, and K. Hirao, "Writing waveguides in glass with a femtosecond laser," Opt. Lett. **21**, 1729–1731 (1996).
2. K. Hirao and K. Miura, "Writing waveguides and gratings in silica and related materials by a femtosecond laser," J. Non-Cryst. Solids **239**, 91–95 (1998).

3. A. M. Streltsov and N. F. Borrelli, "Study of femtosecond-laser-written waveguides in glasses," J. Opt. Soc. Am. B **19**, 2496–2505 (2002).
4. D. M. Krol, "Femtosecond laser modification of glass," J. Non-Cryst. Solids **354**, 416–424 (2008).
5. A. H. Nejadmalayeri and P. R. Herman, "Rapid thermal annealing in high repetition rate ultrafast laser waveguide writing in lithium niobate," Opt. Express **15**, 10842 (2007).
6. T. Allsop, M. Dubov, A. Martinez, F. Floreani, I. Khrushchev, D. J. Webb, and I. Bennion, "Bending characteristics of fiber long-period gratings with cladding index modified by femtosecond laser," J. Lightwave Technol. **24**, 3147–3154 (2006).
7. T. Allsop, K. Kalli, K. Zhou, Y. Lai, G. Smith, M. Dubov, D. J. Webb, and I. Bennion, "Long period gratings written into a photonic crystal fibre by a femtosecond laser as directional bend sensors," Opt. Commun. **281**, 5092–5096 (2008).
8. V. R. Bhardwaj, E. Simova, P. B. Corkum, D. M. Rayner, C. Hnatovsky, R. S. Taylor, B. Schreder, M. Kluge, and J. Zimme, "Femtosecond laser-induced refractive index modification in multicomponent glasses," J. Appl. Phys. **97**, 083102 (2005).
9. S. M. Eaton, M. L. Ng, J. Bonse, A. Mermillod-Blondin, H. Zhang, A. Rosenfeld, and P. R. Herman, "Low-loss waveguides fabricated in BK7 glass by high repetition rate femtosecond fiber laser," Appl. Opt. **47**, 2098–2102 (2008).
10. FEMTOLASERS, Produktions GmbH, Fernkorngasse, Vienna, Austria, http://www.femtolasers.com/.
11. S. M. Eaton, H. Zhang, M. L. Ng, J. Li, W-J. Chen, S. Ho, and P. R. Herman, "Transition from thermal diffusion to heat accumulation in high repetition rate femtosecond laser writing of buried optical waveguides," Opt. Express **16**, 9443–9458 (2008).
12. M. Kalal and K. A. Nugent, "Abel inversion using fast Fourier transforms," Appl. Opt. **27**, 1956–1959 (1988).
13. A. Roberts, E. Ampem-Lassen, A. Barty, K. A. Nugent, G. W. Baxter, N. M. Dragomir, and S. T. Huntington, "Refractive-index profiling of optical fibers with axial symmetry by use of quantitative phase microscopy," Opt. Lett. **27**, 2061–2063 (2002).
14. M. Ams, G. D. Marshall, and M. J. Withford, "Study of the influence of femtosecond laser polarization on direct writing of waveguides," Opt. Express **14**, 13158 (2006).
15. R. Osellame, N. Chiodo, V. Maselli, A. Yin, M. Zavelani-Rossi, G. Cerullo, and P. Laporta, "Optical properties of waveguides written by a 26 MHz stretched cavity Ti:sapphire femtosecond oscillator," Opt. Express, **13**, 612–620 (2005).
16. J. F. Power, "Pulsed mode thermal lens effect detection in the near field via thermally induced probe beam spatial phase modulation: a theory," Appl. Opt. **29**, 52–63 (1990).
17. R. Brückner, "Properties and structure of vitreous silica. I," J. Non-Cryst. Solids **5**, 123–175 (1970).
18. http://www.uqgoptics.com
19. E. R. G. Eckert and R. M. Drake, *Heat and Mass Transfer* (McGraw-Hill, 1959).
20. M. Dubov, T. D. P. Allsop, S. R. Natarajan, V. K. Mezentsev, and I. Bennion, "Low-loss waveguides in borosilicate glass fabricated by high-repetition-rate femtosecond chirp-pulsed oscillator," in *Conference on Lasers and Electro-Optics 2009 and the European Quantum Electronics Conference* (IEEE, 2009), paper CE.P.4 MON.
21. A. W. Snyder and J. D. Love, *Optical Waveguide Theory* (Chapman & Hall, 1991).